Inorganic Chemistry

Article

pubs.acs.org/IC

Oxidation State of Uranium in $A_6Cu_{12}U_2S_{15}$ (A = K, Rb, Cs) Compounds

Christos D. Malliakas,[†] Jiyong Yao,[†] Daniel M. Wells,[†] Geng Bang Jin,[†,‡] S. Skanthakumar,[‡] Eun Sang Choi,[§,⊥] Mahalingam Balasubramanian,[∥] L. Soderholm,[‡] Donald E. Ellis,[†] Mercouri G. Kanatzidis,*[,†] and James A. Ibers*[,†]

[†]Department of Chemistry, Northwestern University, Evanston, Illinois 60208-3113, United States

[‡]Chemical Science and Engineering Division and [∥]Advanced Photon Source, Argonne National Laboratory, Argonne, Illinois 60439, United States

[§]Department of Physics and [⊥]National High Magnet Field Laboratory, Florida State University, Tallahassee, Florida 32310, United States

Supporting Information

ABSTRACT: Black single crystals of $A_6Cu_{12}U_2S_{15}$ (A = K, Rb, Cs) have been synthesized by the reactive flux method. These isostructural compounds crystallize in the cubic space group $Ia\bar{3}d$ at room temperature. The structure comprises a three-dimensional framework built from US_6 octahedra and CuS_3 trigonal planar units with A cations residing in the cavities. There are no S−S bonds in the structure. To elucidate the oxidation state of U in these compounds, various physical property measurements and characterization methods were carried out. Temperature-dependent electrical resistivity measurement on a single crystal of $K_6Cu_{12}U_2S_{15}$ showed it to be a semiconductor. These three $A_6Cu_{12}U_2S_{15}$ (A = K, Rb, Cs) compounds all exhibit small effective magnetic moments, < 0.58 μ_B/U and band gaps of about 0.55(2) eV in their optical absorption spectra. From X-ray absorption near edge spectroscopy (XANES), the absorption edge of $A_6Cu_{12}U_2S_{15}$ is very close to that of UO_3. Electronic band structure calculations at the density functional theory (DFT) level indicate a strong degree of covalency between U and S atoms, but theory was not conclusive about the formal oxidation state of U. All experimental data suggest that the $A_6Cu_{12}U_2S_{15}$ family is best described as an intermediate U^{5+}/U^{6+} sulfide system of $(A^+)_6(Cu^+)_{12}(U^{5+})_2(S^{2-})_{13}(S^-)_2$ and $(A^+)_6(Cu^+)_{12}(U^{6+})_2(S^{2-})_{15}$.

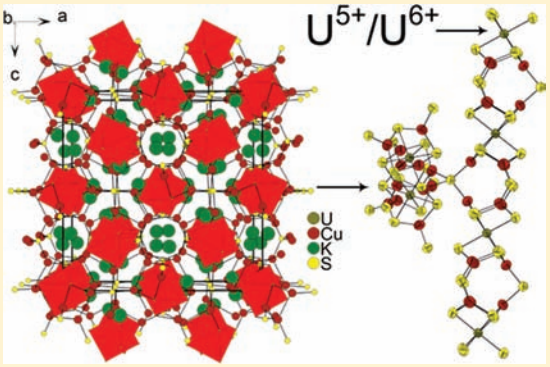

INTRODUCTION

Actinide compounds are of great interest for several reasons. First, their 5f electrons tend to be intermediate between the itinerant 3d or 4d electrons of the transition metals and the more localized 4f electrons of the rare-earth elements. Thus, actinide compounds often exhibit distinct electronic and magnetic behavior.[1−4] Second, in the early actinides, namely, U to Am, and to some extent Cm, the energies of the 7s, 6d, and 5f orbitals are close to degenerate, thus allowing for the possibility of multiple oxidation states.[5−9] For example, the formal oxidation state of U, which is fundamental to understanding its chemistry, can range from +2 to +6. In the past decade, many new ternary and quaternary solid-state actinide chalcogenides have been discovered.[10−13] Many of these contain Q−Q single bonds and short-range Q···Q interactions. In such instances, the assignment of formal oxidation states only on the basis of the structure and stoichiometry is often very difficult, if not impossible. For example, in the AAn_2Q_6 (A = alkali metal; An = actinides, Q = S, Se, Te) family, $K_{0.91}U_{1.79}S_6$ and KU_2Se_6[14] are of the KTh_2Se_6 structure type.[15] Both contain infinite one-dimensional linear Q−Q chains characteristic of this structure type. In $K_{0.91}U_{1.79}S_6$ there are alternating normal S_2^{2-} pairs 2.097(5) Å in length, and the oxidation states of the elements may be assigned as $(K^+)_{0.91}(U^{4+})_{1.79}(S_2^{2-})_2(S^{2-})_2$ and charge balance is achieved. In contrast, in KU_2Se_6 there are two alternating Se···Se distances of 2.703(2) Å and 2.855(2) Å, both much longer than a Se−Se single bond of length 2.34 Å. Here, the oxidation state of U is in question. The assignment of oxidation states is even more complicated in some Cu/S compounds, such as CuS,[16] ACu_4Q_3 (A = alkali metal),[17,18] and $Na_3Cu_4S_4$,[19−21] where metallic conductivity has been interpreted on the basis of holes in the S 3p valence band.

In most of the reported uranium chalcogenides, the oxidation state of U is +4. Reported exceptions include ScU_3S_6,[6] $ScUS_3$,[22] and UTe_2[23] where U is presumably +3, $Rb_4U_4P_4Se_{26}$[24,25] $Tl_3Cu_4USe_6$,[26] and $K_2Cu_3US_5$,[5] where it is +5. To the best of

Received: January 23, 2012
Published: May 14, 2012

   dx.doi.org/10.1021/ic300172k | Inorg. Chem. 2012, 51, 6153−6163

our knowledge there are no reports of hexavalent U-containing chalcogenide compounds. Another reported compound with U in the +5 oxidation state is $K_6Cu_{12}U_2S_{15}$.[27,28] However, preliminary measurements on large single crystals of the isostructural compound $Rb_6Cu_{12}U_2S_{15}$ were not consistent with those made earlier on pressed polycrystalline samples of $K_6Cu_{12}U_2S_{15}$. This observation necessitated a thorough investigation of the $A_6Cu_{12}U_2S_{15}$ (A = K,[27] Rb, Cs) series of compounds. Here, we report their syntheses, structure, transport, optical, magnetic properties, and electronic structures. Unfortunately, these do not lead to an unambiguous elucidation of a single formal oxidation state of U in $A_6Cu_{12}U_2S_{15}$, but taking into account all the experimental information an intermediate U^{5+}/U^{6+} sulfide system is proposed. We also report a low-temperature structural phase transition in $K_6Cu_{12}U_2S_{15}$, which undergoes symmetry reduction with a change of cubic space group from $Ia\bar{3}d$ to $Pa\bar{3}$.

EXPERIMENTAL SECTION

Syntheses. The following reagents were used as obtained: K (analytical reagent, Aldrich Chemical Co., Milwaukee, WI), Rb (Aldrich, 98+%), Cs (analytical reagent, Johnson Matthey/AESAR Group), U (depleted, ORNL), Cu (Aldrich, 99.999%), S (Alfa Aesar, 99.99%), and *N*,*N*-dimethylformamide (DMF, Mallinckrodt Analytical). The reactive fluxes Rb_2S_3 and A_2S (A = K, Cs) were prepared by the stoichiometric reactions of the elements in liquid NH_3.[29] For the syntheses of the K and Cs compounds, Cu metal (40 mesh, Cerac, Milwaukee, WI) was first activated by washing it with copious amounts of dilute hydrochloric acid. This step was necessary to remove the oxide layer from the fine particles (powder) and promote stoichiometric reaction of Cu.

Synthesis of $Rb_6Cu_{12}U_2S_{15}$. The reaction mixtures included Rb_2S_3 (0.1756 g, 0.66 mmol), Cu (0.0356 g, 0.56 mmol), U (0.0224 g, 0.094 mmol), and S (0.0662 g, 2.1 mmol). Reactions were carried out in carbon-coated fused-silica tubes. The tubes were charged with reaction mixtures under an Ar atmosphere in a glovebox. The tubes were evacuated to 10^{-4} Torr and flame-sealed before being placed in a computer-controlled furnace. The reactants were heated to 793 K in 1 d, held at 793 K for 7 d, cooled to 423 K in 8 d, and then cooled to 298 K in 4 h. The products were washed with DMF, and then dried with acetone. From both single crystal and X-ray powder diffraction measurements it was found that the products included black polyhedral-shaped $Rb_6Cu_{12}U_2S_{15}$ crystals, red $RbCuS_4$ long needles,[30] black $RbCu_4S_3$[31] prisms, blue hexagonal CuS[32] plates, and a black powder, which mainly consisted of US[33] and β-US_2.[34] The yield of black polyhedra of $Rb_6Cu_{12}U_2S_{15}$ was about 40 wt % based on Cu. Analysis of several blocks with an EDX-equipped Hitachi S-3500 SEM showed the presence of only Rb, Cu, U, and S.

Synthesis of $K_6Cu_{12}U_2S_{15}$ and $Cs_6Cu_{12}U_2S_{15}$. Mixtures of K_2S (0.721 g, 6.54 mmol) or Cs_2S (1.327 g, 6.54 mmol), activated Cu (0.623 g, 9.81 mmol), U (0.389 g, 1.63 mmol), and S (0.839 g, 26.16 mmol) were loaded into fused-silica tubes under N_2, sealed under vacuum ($<10^{-4}$ Torr), heated to 823 K in 12 h, and held there for 8 d. The tubes were then cooled to 293 K at a rate of 4 K min^{-1}. The excess polychalcogenide flux was dissolved in degassed DMF. The dissolution was performed in an Erlenmeyer flask under flowing N_2 to prevent oxidation of polysulfide to sulfur. Successive portions of DMF were used and decanted until the blue-green solution of the polysulfide remained clear. The final solid product was washed with ether and dried under N_2. From X-ray powder diffraction measurements it was found that the products of the synthesis of $K_6Cu_{12}U_2S_{15}$ included black polyhedral-shaped crystals of the target compound, dark blue plate-like crystals of KCu_4S_3,[31] and UOS.[33] The yield of black polyhedra of $K_6Cu_{12}U_2S_{15}$ was about 70 wt % based on Cu. The products of the synthesis of $Cs_6Cu_{12}U_2S_{15}$ were mainly black polyhedral-shaped crystals of the target compound and a fraction of about 5 wt % of US[33] impurities. Analysis of several crystals with an EDX-equipped Hitachi S-3500 SEM showed the presence of alkali metal (Rb or Cs), Cu, U, and S at the expected stoichiometry. No evidence of decomposition or oxidation was present on $K_6Cu_{12}U_2S_{15}$ by single crystal X-ray diffraction measurements. The sample was kept in air (ambient conditions) for a period of around two months.

Structure Determinations. Single-crystal X-ray diffraction data from $Rb_6Cu_{12}U_2S_{15}$ were collected with the use of graphite-monochromatized Mo Kα radiation (λ = 0.71073 Å) on a Bruker Smart-1000 CCD diffractometer. The crystal-to-detector distance was 5.023 cm. Crystal decay was monitored by recollecting 50 initial frames at the end of data collection. No obvious crystal decay was observed. Data were collected by a scan of 0.3° in ω in groups of 606 frames at φ settings of 0°, 90°, 180°, and 270° with an exposure time of 15 s/frame. The collection of the intensity data was carried out with the program SMART.[35] Cell refinement and data reduction were carried out with the use of the program SAINT,[35] and a face-indexed absorption correction was performed numerically with the use of the program XPREP.[36] Then the program SADABS[37] was employed to make incident beam and decay corrections.

Intensity data from $K_6Cu_{12}U_2S_{15}$ and $Cs_6Cu_{12}U_2S_{15}$ were collected on a STOE IPDS II diffractometer equipped with graphite monochromatized Mo radiation (λ = 0.71073 Å) and an Image Plate (IP) detector. The data were collected with an ω-scan technique from 0−180° at an arbitrary φ-angle. Data reduction was performed with the X-AREA package.[38] An analytical absorption correction was performed (X-SHAPE2 within X-AREA).

The structures were solved with the direct-methods program SHELXS and refined with the least-squares program SHELXL.[39] The program STRUCTURE TIDY[40] was then employed to standardize the atomic coordinates in the structures. Additional experimental details are given in Table 1 and in the Supporting Information. Selected metrical data are given in Table 2.

Table 1. Crystal Data and Structure Refinements for $A_6Cu_{12}U_2S_{15}$ (A = K, Rb, Cs)[a]

	$K_6Cu_{12}U_2S_{15}$	$K_6Cu_{12}U_2S_{15}$	$Rb_6Cu_{12}U_2S_{15}$	$Cs_6Cu_{12}U_2S_{15}$
Fw	1954.31	1954.31	2232.26	2516.90
a (Å)	18.5520(3)	18.6208(7)	18.8064(5)	19.0217(6)
V (Å^3)	6385.17(18)	6456.5(4)	6651.5(3)	6882.5(4)
T (K)	100(3)	300(3)	153(2)	100(3)
space group	$Pa\bar{3}$	$Ia\bar{3}d$	$Ia\bar{3}d$	$Ia\bar{3}d$
ρ_c (g cm^{-3})	4.066	4.020	4.458	4.858
μ (cm^{-1})	196.76	194.58	268.62	237.84
$R(F)^b$	0.0457	0.0481	0.0258	0.0362
$R_w(F_o^2)^c$	0.1185	0.1363	0.0645	0.0651
m^d	0.0481	0.0496	0.02	0.0125
n^d	128.6468	383.4168	150	288.3029

[a]For all structures Z = 8, and λ = 0.71073 Å. [b]$R = \sum||F_o| - |F_c||/\sum|F_o|$ for $F_o^2 > 2\sigma(F_o^2)$. [c]$R_w = (\sum[w(|F_o|^2 - |F_c|^2)^2]/\sum[w(|F_o|^4)])^{1/2}$ for all data. [d]$w = 1/[\sigma^2(F_o^2) + (mP)^2 + nP]$ and $P = (F_o^2 + 2F_c^2)/3$.

Interestingly, $K_6Cu_{12}U_2S_{15}$ undergoes a phase transition at low temperature. The space group symmetry decreases from $Ia\bar{3}d$ to $Pa\bar{3}$ along with formation of second twin domain at 100 K. A twin law [0 −1 0 −1 0 0 0 0 1] of 90 degrees rotation along the *c*-axis was used with a refined twin fraction of 58.3(1)%. The coordination environment of all atoms is distorted with respect to the 300 K structure, as is shown in Table 2 and in the Supporting Information. Given the isostructural character of the $A_6Cu_{12}U_2S_{15}$ (A = K, Rb, Cs) system at room temperature we suspect that there must be a structural transition present for both the Rb and the Cs analogues that depends on the size of the alkali metal. Since $Cs_6Cu_{12}U_2S_{15}$ did not show a structural transition down to 100 K the transition temperature must be below 100 K, but unfortunately we could not perform the diffraction experiment at such low temperature to confirm this hypothesis.

Electrical Resistivity Measurements on $K_6Cu_{12}U_2S_{15}$. Numerous attempts to attach contacts directly to the surface of single crystals with silver paint gave no reading at 293 K on a ~10 GΩ voltmeter.

dx.doi.org/10.1021/ic300172k | Inorg. Chem. 2012, 51, 6153−6163

Table 2. Selected Interatomic Distances (Å) for $A_6Cu_{12}U_2S_{15}$ (A = K, Rb, Cs)

	$A_6Cu_{12}U_2S_{15}$ (A = K, Rb, Cs) in Space Group $Ia\bar{3}d$		
	$K_6Cu_{12}U_2S_{15}$ at 300 K	$Rb_6Cu_{12}U_2S_{15}$ at 153 K	$Cs_6Cu_{12}U_2S_{15}$ at 100 K
U−S1 × 6	2.615(3)	2.612(1)	2.598(2)
Cu−S1	2.240(3)	2.244(2)	2.249(2)
Cu−S1	2.244(3)	2.253(2)	2.251(2)
Cu−S2	2.200(1)	2.2172(7)	2.2312(9)
	$K_6Cu_{12}U_2S_{15}$ at 100 K in Space Group $Pa\bar{3}$		
U1−S4 × 2	2.621(2)	Cu1−S3	2.244(2)
U1−S4	2.622(2)	Cu2−S1	2.197(2)
U1−S5 × 3	2.608(2)	Cu2−S4	2.237(2)
U1−S4 × 2	3.8406(5)	Cu2−S4	2.242(2)
U2−S2 × 6	2.614(2)	Cu3−S1	2.207(2)
U3−S3 × 6	2.610(2)	Cu3−S5	2.232(2)
Cu1−S1	2.196(2)	Cu3−S5	2.243(2)
Cu1−S3	2.239(2)		

Considering the relatively narrow band gap of ∼0.55 eV (see below) we would expect a resistivity value of less than 10 GΩ·cm. Because we suspected surface oxidation and formation of an insulating protective layer, we used a combination of in situ sputtering and deposition of ∼5 Å of Cr and ∼50 Å of Au to protect the surface of one side of length ∼500 μm of a polished single crystal. Four Cu leads (∼ 25 μm in diameter) were attached in series and electrical contact was made with Ag paint. A FEI Helios NanoLab Dual Beam Focused-Ion-Beam (FIB)/Scanning Electron Microscope (SEM) was used to ion-mill the Cr and Au located between the Cu wires. Measurements from 2 to 300 K were made for arbitrary current directions with the use of standard four-point contact geometry (AC) in a Quantum Design Physical Property Measurement System (PPMS).

Magnetic Susceptibility Measurements. Magnetic susceptibility data were collected with the use of a Quantum Design MPMS 7 SQUID magnetometer. The empty sample holder, which contributed significantly to the output signal, was measured separately, the results were directly subtracted from the total signal obtained from sample plus holder, and a Langevin diamagnetic correction was applied. Data were collected on several samples of $A_6Cu_{12}U_2S_{15}$ (A = K, Rb, and Cs), each of which was composed of many small single crystals. These samples were obtained by grinding numerous, hand-selected single crystals. The phase purity of each sample was checked by an X-ray powder diffraction measurement; the pattern showed no extra lines.

Variable field measurements, performed at 40 and 300 K to a maximum field of 1 T, appeared linear over the entire range, thus enabling data acquisition at higher fields. Field-cooled and zero-field-cooled data showed small differences only below 20 K. When combined with variable field measurements obtained at 2 K, the data indicate a small ferromagnetic component (less than $1 \times 10^{-4} \mu_B$) in samples of all three compounds at low temperatures. Very small amounts of contaminant are commonly suspected in the synthetic approach used here and are observable in systems with small intrinsic moments.[41−43] However, for the present sulfide samples the observed hysteresis, used to quantify the presence of a ferromagnetic impurity, has disappeared by 40 K, ruling out a simple Fe impurity. Variable temperature experiments were carried out between 2 and 320 K, under applied fields of 0.05, 0.1, 0.2, 0.5, and 1 T, all of which provided reproducible data above 20 K.

X-ray Absorption Near Edge Spectroscopy (XANES). X-ray absorption near-edge spectroscopy (XANES) experiments were performed in Sector 20, bending magnet beamline (PNC/XOR, 20-BM) of the Advanced Photon Source at the Argonne National Laboratory. Measurements at the U L_{III} edge and at ambient temperature and pressure were performed in the transmission mode with the use of gas ionization chambers to monitor the incident and transmitted X-ray intensities. A third ionization chamber was used in conjunction with a uranyl nitrate standard sample to provide internal calibration for the alignment of the edge positions. Monochromatic X-rays were obtained with the use of a Si (111) double crystal monochromator. A Rh-coated X-ray mirror was utilized to suppress higher order harmonics.

The $K_6Cu_{12}U_2S_{15}$, $Rb_6Cu_{12}U_2S_{15}$, $Cs_6Cu_{12}U_2S_{15}$, β-US_2,[34] UO_2,[44] and UO_3[45] samples were prepared by mixing an appropriate amount of single crystals of each sample with BN powder (to minimize self-absorption) and packing them into Teflon holders (2 × 10 mm slot) that were then sealed with Kapton tape. Data reduction and analysis were performed with the ATHENA software.[46]

Band-Gap Measurement. Optical diffuse reflectance measurements were performed at 293 K with a Shimadzu UV-3101 PC double-beam, double-monochromator spectrophotometer operating in the 200−2500 nm region. The computer-controlled instrument was equipped with an integrating sphere. $BaSO_4$ was used as a 100% reflectance standard. The sample was prepared by grinding the crystals to a powder that was then spread on a compacted bed of $BaSO_4$ powder standard material. The generated reflectance-versus-wavelength data were used to estimate the band gap of the material by converting reflectance to absorption data according to the Kubelka−Munk equation: $\alpha/S = (1 - R)^2/(2R)$, where R is the reflectance and α and S are the absorption and scattering coefficients, respectively.[47−49]

Calculated Electronic Structures: Methodology. Periodic spin-polarized band-structure calculations were performed on the structure of $A_6Cu_{12}U_2S_{15}$ (A = Rb, K) using the first-principles density functional theory (DFT) program VASP (Vienna ab initio Simulation Package) in which pseudopotentials with a plane-wave basis were applied.[50−53] The exchange-correlation potential was chosen as the generalized gradient approximation (GGA) in a projector augmented wave (PAW) method developed by Kresse and Joubert.[54] Automatically generated Monkhorst-Pack grids were used to carry out Brillouin zone integrations.[55] 4 × 4 × 4 k-point meshes were chosen for relaxations; these were increased to 6 × 6 × 2 for establishing convergence and density of states (DOS) analysis.

On-site Coulomb corrections (Hubbard U)[56] for the U 5f electrons were included (so-called LDA+U method) as they significantly impact the distribution of occupied states for heavy elements. This method was included in final calculations of charge distribution, magnetic moments, and DOS, but was not used during atomic relaxations as it is expected to have little effect on the atomic positions. The on-site Coulomb interaction was handled by the method of Dudarev et al.[57] where the effective Coulomb interaction U and the effective exchange interaction J are combined as a single term $U_{eff} = U - J$. The calculated values for atomic U ($5f^3$) are U = 2 eV, J = 0.55 eV,[58,59] but to achieve a fit to physical property data these values had to be greatly reduced.[60−62] In the current calculations, a range of values U_{eff} = 1, 2, and 4 eV was used to explore its effects on properties.

The electrons described as core in the projector augmented-wave (PAW) potentials are those comprising [Ne]/[Ar] for K/Rb leaving 7 valence electrons per atom as $4p^6 5s^1$; [Ar] for Cu leaving 11 valence electrons per atom as $3d^{10}4s^1$; [Xe]$5d^{10}4f^{14}$ for U leaving 14 valence electrons per atom as $5f^3 6s^2 6p^6 6d^1 7s^2$; and [Ne] for S leaving 6 valence electrons per atom as $3s^2 3p^4$. Oxidation states were investigated by means of electronic charges determined by spherical volume integration over "Wigner−Seitz radii" R_{ws}. The difference between the number of valence electrons contained within a volume and the number assigned to the neutral atom is defined here as one measure of the oxidation state. The values of R_{ws} were initially set to the standard crystal radii[63] and were increased to maximize the cell volume included within the spheres while maintaining the proportionality of each volume type. The final radii used were 2.05 Å for Rb, 1.1 Å for Cu, 1.35 Å for U, and 2.05 Å for S. An alternative set with radius 1.1 Å for Rb was used to explore its charge localization. The Bader topological atoms procedure,[64] which integrates the electronic charge within zero-flux surfaces surrounding atoms, was also applied to obtain further insight about the atomic valence states.

dx.doi.org/10.1021/ic300172k | Inorg. Chem. 2012, 51, 6153−6163

RESULTS AND DISCUSSION

Syntheses. From X-ray powder diffraction measurements it was found that the yield of $Rb_6Cu_{12}U_2S_{15}$ crystals was about 40% based on Cu. By-products included red $RbCuS_4$ long needles, black $RbCu_4S_3$ prisms, blue hexagonal CuS plates, and a black powder, which mainly consisted of US and US_2. The yield of the black polyhedral $K_6Cu_{12}U_2S_{15}$ crystals was about 70 wt % based on Cu, with KCu_4S_3 and UOS impurities. Under the same synthetic conditions (temperature and time) the $Cs_6Cu_{12}U_2S_{15}$ system gave black polyhedral crystals. Only a small fraction (~5%) of US impurities was present. Analysis of several crystals of each compound with an EDX-equipped Hitachi S-4200 SEM confirmed the presence of all elements at the expected ratio.

Structures. The isostructural $A_6Cu_{12}U_2S_{15}$ (A = K, Rb, Cs) compounds crystallize with eight formula units in space group $Ia\bar{3}d$ of the cubic system at room temperature with a cuboctahedral crystal habit (Figure 1). The new structure

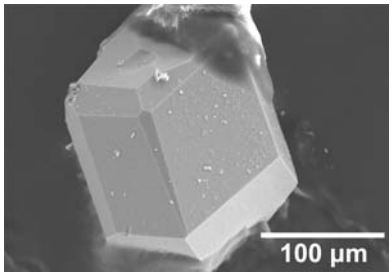

Figure 1. SEM picture of the single crystal of $Cs_6Cu_{12}U_2S_{15}$ that was used for the X-ray diffraction experiment.

type has been described in detail earlier.[27] In the asymmetric unit there is one crystallographically unique A atom at a site with 2 symmetry, one unique Cu atom at a general site, one unique U atom at a site with symmetry $\bar{3}$, and two unique S atoms, one at a general site and the other at a site of $\bar{4}$ symmetry. Each A atom is coordinated by a bicapped trigonal prism of eight S atoms; the U atom is coordinated by an octahedron of six S atoms; and the Cu atom is coordinated by a trigonal planar unit of three S atoms.

The structure of $A_6Cu_{12}U_2S_{15}$ is shown in Figure 2. Its three-dimensional cubic framework is built from US_6 octahedra and CuS_3 trigonal planar units with A cations residing in the cavities. The basic building block can be viewed as a fragment composed of one US_6 octahedron and six CuS_3 trigonal planar units (Figure 3). The US_6 octahedron edge shares with each CuS_3 unit. Four such building blocks are connected to each other by Cu−S2 interactions. Each S1 atom is coordinated to two Cu atoms and one U atom within the building block. The complex connection of these basic building blocks extends in all three directions to produce the cubic structure.

Selected interatomic distances for $A_6Cu_{12}U_2S_{15}$ are listed in Table 2. The U−S distance is 2.615(3) Å in $K_6Cu_{12}U_2S_{15}$, 2.612(1) Å in $Rb_6Cu_{12}U_2S_{15}$, and 2.598(2) Å in $Cs_6Cu_{12}U_2S_{15}$. These distances are close to each other, but shorter than a typical U^{4+}−S distance (for example, 2.680(5) to 2.709(5) Å in $BaUS_3$).[65,66] The Cu−S distances are 2.200(1), 2.240(3), and 2.244(3) Å in $K_6Cu_{12}U_2S_{15}$, 2.2172(7), 2.244(2), and 2.253(2) Å in $Rb_6Cu_{12}U_2S_{15}$, and 2.2312(9), 2.246(2), and 2.251(2) Å in $Cs_6Cu_{12}U_2S_{15}$, comparable to those of 2.245(3) Å for trigonal-planar coordinated Cu in $CsCuTeS_3$.[67] The K−S distances range from 3.261(4) to 3.554(3) Å, consistent with those of

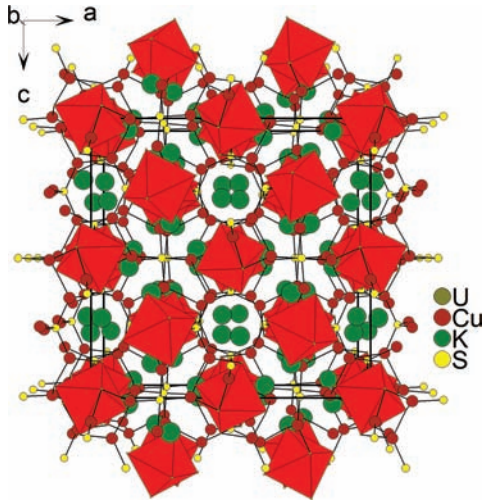

Figure 2. Perspective view along [010] of the unit cell of the $A_6Cu_{12}U_2S_{15}$ structure at room temperature. US_6 octahedra are shown in red polyhedra.

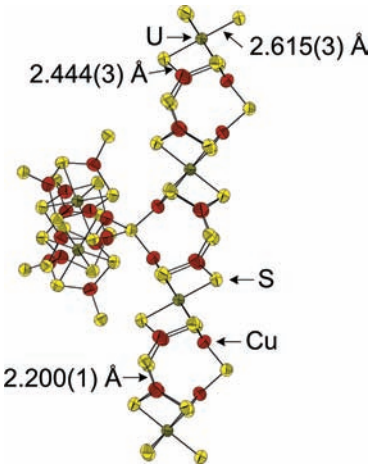

Figure 3. Four basic building blocks of the $A_6Cu_{12}U_2S_{15}$ structure (the displacement ellipsoids are drawn at the 90% probability level).

3.190(3) to 3.585(2) Å in $KCuUS_3$,[9] the Rb−S distances range from 3.315(2) to 3.4003(14) Å, comparable to those of 3.293(2) to 3.460(1) Å in $RbHo_2Cu_3S_5$,[68] the Cs−S distances range from 3.387(2) to 3.8868(4) Å, close to those of 3.432(2) to 3.890(2) Å in $CsBiGeS_4$.[69]

There are no S−S bonds in the structure of $A_6Cu_{12}U_2S_{15}$, the shortest S···S distance being 3.616(2) Å in $K_6Cu_{12}U_2S_{15}$. To achieve charge balance, there are three possible models for formal oxidation states: $(K^+)_6(Cu^+)_{12}(U^{4+})_2(S^{2-})_{11}(S^-)_4$, $(K^+)_6(Cu^+)_{12}(U^{5+})_2(S^{2-})_{13}(S^-)_2$, and $(K^+)_6(Cu^+)_{12}(U^{6+})_2(S^{2-})_{15}$ on the assumption that Cu^{2+} is too oxidizing to exist in sulfide-containing compounds. The first two $U^{4+}$and U^{5+} models assume that there are holes in the S 3p valence bands and therefore the compounds should be p-type metals with large remaining magnetic moments on U, whereas for the U^{6+} model the compounds should be semiconducting and diamagnetic. Thus physical property measurements were essential to a further exploration of these models.

Semiconducting Gap and Electrical Resistivity. All three $A_6Cu_{12}U_2S_{15}$ (A = K, Rb, Cs) compounds are semiconductors at 293 K with a gap of 0.55(2) eV, as can be

dx.doi.org/10.1021/ic300172k | Inorg. Chem. 2012, 51, 6153−6163

seen by the optical absorption spectra in Figure 4. The gap barely changes with the alkali metal.

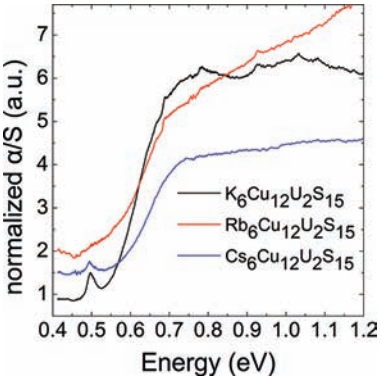

Figure 4. Room-temperature optical absorption spectra of $A_6Cu_{12}U_2S_{15}$ (A = K, Rb, Cs) showing a band gap of 0.55(2) eV.

The peak before the absorption edge can be assigned to an electronic transition between the 5f and 6d orbitals of the U atoms, and it is typical for a uranium-containing compound.[70] The $Rb_6Cu_{12}U_2S_{15}$ sample was the most impure sample in the $A_6Cu_{12}U_2S_{15}$ series, and this is also reflected in the absorption spectrum with a shoulder below the absorption edge. The electronic transition peak must be there in the $Rb_6Cu_{12}U_2S_{15}$ curve, but it is hidden under the intensity of the shoulder observed below 0.6 eV. Because of the impurity shoulder the steepness of the absorption edge for $Rb_6Cu_{12}U_2S_{15}$ is also different.

The temperature-dependent single-crystal resistivity data for a sample of $K_6Cu_{12}U_2S_{15}$ confirmed the semiconducting behavior (Figure 5a). The resistivity varies from ∼15 KΩ cm

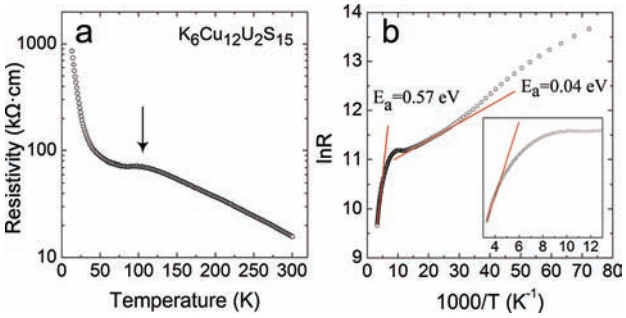

Figure 5. (a) Temperature-dependent resistivity data for $K_6Cu_{12}U_2S_{15}$ showing semiconducting behavior. (b) Arrhenius plot of the resistivity of $K_6Cu_{12}U_2S_{15}$. Red solid lines represent linear fits.

at 300 K to more than 1 MΩ cm at 2 K. The Arrhenius plot of $K_6Cu_{12}U_2S_{15}$ does not show a linear behavior, which suggests that the carrier thermal excitation does not follow a simple mechanism (Figure 5b). There are two apparent activation energies: one in the temperature region of 100−300 K at ∼0.57 eV and the other in the range of 4−80 K at ∼0.04 eV. The former is in good agreement with the observed optical absorption gap of 0.55(2) eV (see above). Interestingly, a change in the slope of the resistivity data was observed at around 100 K, Figure 5a (shown with an arrow). This anomaly may be associated with the phase change that was observed for $K_6Cu_{12}U_2S_{15}$ by the single crystal X-ray diffraction study.

Magnetic Susceptibility. The magnetic responses from all three sulfides were sample dependent, even for different batches of ostensibly the same sample. All compounds except one of the $K_6Cu_{12}U_2S_{15}$ samples discussed below showed a temperature-dependent magnetic behavior. The measurements on the one exception, shown in Figure 6, were made on one

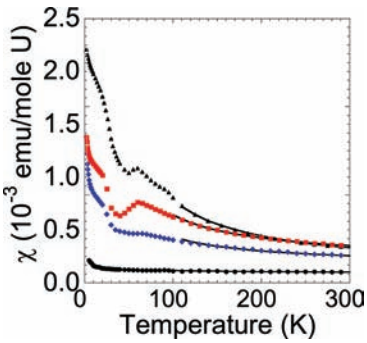

Figure 6. Measured susceptibility as a function of temperature for two K, one Rb, and Cs samples of $A_6Cu_{12}U_2S_{15}$ (K, black circles and triangles; Rb, blue diamonds; Cs, red squares). The black lines through the data represent the best fits (over the temperature range of 100−310 K) from which the effective moments and temperature-independent-paramagnetic contributions were obtained.

26.2 mg $K_6Cu_{12}U_2S_{15}$ sample. Similar to the other samples, it too showed no impurity lines in the X-ray powder pattern, and exhibited no significant measurable temperature-dependent susceptibility. However, the magnetic response as a function of temperature exhibited only a small temperature-independent susceptibility (TIP) over the entire temperature range. Such a TIP response is considered intrinsic to the sample stoichiometry as written. The absence of a temperature-dependent susceptibility rules out even a small contribution from U^{5+}, which has an f^1 configuration and therefore is a Kramers ion; as such it will have a magnetic ground state. Technical difficulties in obtaining the susceptibility data that arise in part from safety concerns associated with handling a radionuclide, notably the use of only small sample sizes and the requirement for encapsulation, which contributes to the background, render it not possible to determine within error limits whether the U sublattice is diamagnetic (U^{6+}) or exhibits a positive signal consistent with a TIP. The presence of Cu in these materials further complicates the issue because it can contribute to a TIP response.[71,72] A large TIP could indicate the stoichiometric presence of U^{4+}. A solely TIP response has been previously observed at higher temperatures (60−300 K) for $BaUO_3$, a tetravalent U ion octahedrally coordinated with six oxygen atoms in full cubic symmetry.[73] The first excited state U^{4+} has an f^2 configuration, which in the Russell−Saunders coupling scheme corresponds to a $^3H_4$ ground term. In octahedral symmetry the ground term is split into one singlet, one doublet, and two triplets, with a Γ_1 singlet as the ground state.[74] TIP over the entire temperature range was not observed for any other A = K sample nor for the A = Rb or Cs analogues.

Notwithstanding the TIP response seen for one of the $K_6Cu_{12}U_2S_{15}$ samples and the considerable variability in the measured susceptibilities for all of the samples, a similarity did emerge in overall magnetic behavior that extended across all three alkali-metal analogues. Representative magnetic susceptibility data from $A_6Cu_{12}U_2S_{15}$ (A = K, Rb, Cs), obtained as a function of temperature and corrected for diamagnetism,

dx.doi.org/10.1021/ic300172k | Inorg. Chem. 2012, 51, 6153−6163

shown in Figure 6, were collected on 30.4, 15.0, and 22.5 mg samples of $K_6Cu_{12}U_2S_{15}$, $Rb_6Cu_{12}U_2S_{15}$, and $Cs_6Cu_{12}U_2S_{15}$, respectively. The samples exhibit a temperature-dependent susceptibility over the entire measured temperature range, which above 100 K can be fit with a modified Curie law $\chi = C/T + \chi_0$,where C is the Curie constant from which the effective magnetic moment is related by $\mu_{eff} = (8C)^{1/2}$, and χ_0 is the TIP. Demonstrated in Figure 7a–c, in which the data are replotted

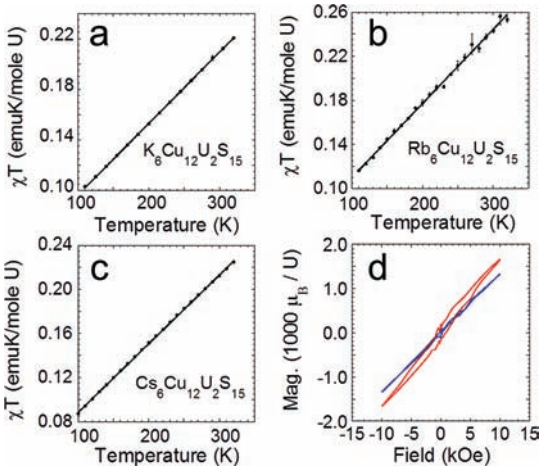

Figure 7. Magnetic susceptibilities plotted as χT versus T to emphasize the importance of the temperature-independent-paramagnetic term, represented by the slope in these plots for (a) $K_6Cu_{12}U_2S_{15}$, (b) $Rb_6Cu_{12}U_2S_{15}$, and (c) $Cs_6Cu_{12}U_2S_{15}$. The linearity of the plots confirms the absence of a significant Weiss constant for these data. The line through the data represents the best fit, discussed in the text. (d) The hysteresis of $K_6Cu_{12}U_2S_{15}$ at 2 K (red) and 40 K (blue). The data, which are similar to those reported previously for U^{5+} in KUO_3,[77] suggest a ferromagnetic ordering below 40 K.

as χT versus T and compared with calculated values based on the best fit, there is no evidence of a significant Weiss contribution. When warranted, a Weiss constant is used to account for variations in a simple paramagnetic response arising from either low-lying crystal-field states or magnetic correlations. There is no evidence to support such behavior, despite the anomalies in the magnetic responses around 50 and 20 K. The results of the data fitting are shown in Table 3.

The magnitude of the observed effective moments for the three samples is too large to result from a magnetic impurity phase and thus eliminates from consideration the simple $(A^+)_6(Cu^+)_{12}(U^{6+})_2(S^{2-})_{15}$ model for U–S charge distribution. The susceptibility response at low temperature does not

Table 3. Average Results From Fits to the Magnetic Susceptibilities of $A_6Cu_{12}U_2S_{15}$ (A = K, Rb, Cs) Samples Under a 0.5 T Magnetic Field

compound	weight (mg)	μ_{eff} (μ_B/mol U)[a]	μ_{TIP} (emu/mol U)
$K_6Cu_{12}U_2S_{15}$	26.2	0.0(1)	5.6×10^{-4}
$K_6Cu_{12}U_2S_{15}$	30.4	0.57(5)	5.6×10^{-4}
$Rb_6Cu_{12}U_2S_{15}$	6.8	0.58(5)	6.7×10^{-4}
$Rb_6Cu_{12}U_2S_{15}$	15.0	0.36(10)	6.0×10^{-4}
$Cs_6Cu_{12}U_2S_{15}$	22.5	0.46(10)	6.2×10^{-4}

[a]The effective moments (μ_{eff}) were obtained by fitting the χ vs T data over the temperature range 100–320 K. The fits are shown as solid lines through the data in Figure 6.

strongly support the presence of tetravalent uranium, as would be found in model $(A^+)_6(Cu^+)_{12}(U^{4+})_2(S^{2-})_{11}(S^-)_4$, although it does not strictly eliminate it. The charge distribution that results in pentavalent uranium, that is, $(A^+)_6(Cu^+)_{12}(U^{5+})_2(S^{2-})_{13}(S^-)_2$, appears most consistent with the magnetic data. U^{5+} has an f^1 configuration and is expected to follow Russell–Saunders coupling rules, with $L = 3$, $S = 1/2$, and $J = 5/2$ and a $^2F_{5/2}$ ground term. The 6-fold degenerate term is split into a Γ_7 doublet and a Γ_8 quartet by an octahedral crystal field, with the doublet as the ground state[74] and the first excited state high enough in energy not to contribute to the first-order, temperature-dependent, magnetic response.[75,76] The full free-ion effective moment for an f^1 system assuming pure Russell–Saunders coupling is 2.54 μ_B. The effective moment calculated assuming a Γ_7 ground-state doublet, which is composed of mixed $|m_j\rangle$ states $|5/2\rangle$ and $|3/2\rangle$, is 1.24 μ_B, assuming only electrostatic interactions with no interatomic orbital mixing or bonding.[74] Thus our experimentally determined moment of about 0.5 μ_B is much smaller than expected strictly based a comparison with a calculated U^{5+} ion in an octahedral crystal field.

The temperature dependence of the susceptibilities determined experimentally for all three of the complex sulfides show marked similarities to other reports on f^1 systems in octahedral symmetry, including low values of the effective moments. For example, magnetic and neutron diffraction studies on KUO_3, a cubic perovskite in which U^{5+} is octahedrally coordinated to six oxygen atoms, exhibits a temperature dependence to its susceptibility that is very similar to the sulfides studied here.[77] A broad feature centered near 60 K, which is similar to our systems, and a sharp maximum are observed in χ versus T at 17 K, although the low-temperature feature is less well-defined in the sulfides. A similar low-temperature maximum in the susceptibility was also seen in $NaUO_3$,[78] and together with heat capacity measurements[79] was used to assign it to a ferromagnetic transition. Hysteresis measurements on the KUO_3 did show evidence of magnetic ordering at low temperature, but ordering could not be confirmed by neutron diffraction measurements.[77] As demonstrated in Figure 7d the sulfides also show evidence of a weak hysteresis at low temperature. In a $4f^1$ perovskite $BaPrO_3$ there are also clear indications from susceptibility measurements for a magnetic ordering at 11.6(1) K, although it has not been confirmed by neutron diffraction studies.[80]

For temperatures above the broad anomalies in the susceptibilities of the sulfide materials, the effective moment was determined to be about 0.5 μ_B. Reduced moments are relatively common for f^1 systems in six coordinate sites.[81] For example, studies on AUO_3 (A = K, Rb) report effective moments of about 0.66 μ_B,[76,77] and $BaPrO_3$ has an measured effective moment of 0.7(1) μ_B.[80] Electron paramagnetic resonance studies on Pr^{4+} in $BaCeO_3$ support these results.[82] A causal analysis for the experimental determination of a moment that is significantly less than predicted for an f^1 configuration in a octahedral crystal field showed that contributions to the measured susceptibilities resulted from mixing of states arising from the $^2F_{7/2}$ excited term.[80] Although about 3000 cm^{-1} higher in energy than the ground term, a relaxation of the Russell–Saunders formalism that permits intermediate coupling, was an option not available within the Steven's formalism[83] used for the determination of a Γ_7 effective moment of 1.24 μ_B.[74] If one uses all the states within an f^1 configuration and an intermediate coupling scheme, it is

dx.doi.org/10.1021/ic300172k | Inorg. Chem. 2012, 51, 6153–6163

possible to account for an effective moment of 0.5 μ_B for an f^1 system.

The temperature-dependent magnetic behavior observed for $A_6Cu_{12}U_2S_{15}$ (A = K, Rb, Cs) is consistent with a charge distribution corresponding to $(A^+)_6(Cu^+)_{12}(U^{5+})_2(S^{2-})_{13}(S^-)_2$ for all three materials. There is no need to invoke nonstoichiometry or intermediate valence arguments. However, it must be stressed that one of the $K_6Cu_{12}U_2S_{15}$ samples showed only TIP down to the lowest temperatures measured, which is inconsistent with the presence of U^{5+}. Note also that there was considerable scatter in the susceptibility data, particularly in the measured effective moments. Furthermore, no anomalies were observed in the magnetic susceptibility data for $K_6Cu_{12}U_{12}S_{15}$ from the phase change at ~100 K that was observed by single-crystal X-ray diffraction and confirmed by temperature-dependent electrical resistivity measurements. These findings suggest that there may be an interesting valence instability in these materials that has yet to be understood.

X-ray Absorption Near-Edge Spectroscopy (XANES). X-ray absorption near-edge spectroscopy (XANES) has been widely used for the assessment of formal oxidation states of elements in a variety of compounds. The position of the near-edge absorption peak depends mainly on the oxidation state of the absorbing element, and the shape of the pre-edge region depends mainly on the coordination geometry and environment of that element in the crystal structure. Comparison of the position of the near-edge peak with the one of a reference material (a standard compound that has a well-defined oxidation state and similar chemical character) is typically used for the assignment of an oxidation state.

Unfortunately, it appears that no reports of U^{6+} compound exist where the metal is surrounded by a full set of sulfide ligands that can be used as a XANES reference. Therefore we used UO_3 as a reference. As a U^{4+} standard we used US_2 and compared it against UO_2. The XANES spectra are shown in Figure 8, and their fitting parameters are summarized in Table

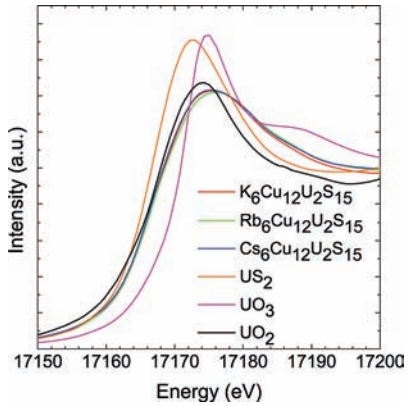

Figure 8. XANES spectra for the $A_6Cu_{12}U_2S_{15}$ family in comparison to US_2, UO_2, and UO_3.

4. All XANES spectra for the $A_6Cu_{12}U_2S_{15}$ (A = K, Rb, Cs) members are identical and group around 17175 eV, verifying the same oxidation state of U and the isostructural nature of the compounds. US_2 has a very different absorption edge position that peaks at around 17172 eV, almost the same as that of UO_2. Therefore, we can rule out the possibility of having U^{4+} in $A_6Cu_{12}U_2S_{15}$. Indeed, the absorption edge of $A_6Cu_{12}U_2S_{15}$ is very close to that of UO_3. Taking into account the ~2 eV

Table 4. Fit Parameters of the Peaks Observed by X-ray Absorption Near-Edge Spectroscopy

	Lorentzian peak		step function	
compound	center (eV)	width (eV)	center (eV)	width (eV)
$K_6Cu_{12}U_2S_{15}$	17174.8(3)	17.9(3)	17167.3(4)	6.2(1)
$Rb_6Cu_{12}U_2S_{15}$	17175.3(3)	18.8(3)	17167.1(4)	6.3(1)
$Cs_6Cu_{12}U_2S_{15}$	17174.6(3)	18.8(4)	17166.4(4)	6.3(1)
US_2	17172.4(3)	13.0(2)	17167.7(3)	5.3(2)
UO_3	17174.6(3)	7.7(2)	17166.4(11)	9.5(3)
UO_2	17172.7(3)	13.3(2)	17166.4(4)	10.2(3)

relative difference between the UO_2 and UO_3 edge and the match of positions between US_2 and UO_2 we find that the edge of $A_6Cu_{12}U_2S_{15}$ is closer to a U^{6+}, though this assignment is tentative owing to the absence of U^{6+}-sulfide and U^{5+}-sulfide XANES standards. A small contribution from U^{5+} centers therefore cannot be excluded. Additionally, the considerably broader width of around 18 eV (Table 4) for the $ACu_{12}U_2S_{15}$ XANES peak in comparison with the narrower 7.7 eV UO_3, and 13 eV UO_2 and US_2 peaks supports the intermediate-valent description.

ELECTRONIC STRUCTURE OF $Rb_6Cu_{12}U_2S_{15}$

Relaxation and Atomic Magnetization. Because the full cubic unit cell (V = 6651.5 Å^3) of the Rb compound contains 280 atoms and 2336 valence electrons, an idealized 140-atom reduced unit cell of the 153 K cubic cell was used for all calculations to reduce the computational burden. The lattice constants of the reduced cell for the Rb compound are $a = b = c$ = 16.287 Å and $\alpha = \beta = \gamma$ = 109.47°. Ionic relaxations were conducted in this fixed unit cell and convergence was established when Hellmann−Feynman forces on each ion fell below 0.02 eV/Å. Calculations were conducted with constrained body-centered cubic symmetry; atomic positions were relaxed, whereas unit cell constants were not varied.

In preliminary calculations without atomic relaxation, the magnetic moment on the U ions within the GGA formalism was found to be approximately 2.7 μ_B with a moment of 0.1 μ_B on the Cu and S ions. The U ions were found to have an electronic configuration of $5f^{3.6}6d^{0.72}$ corresponding to an oxidation state of +2.5, according the R_{WS} volume integration. It is typical that volume integrations yield effective oxidation states very far from the nominal expected (here +4/+5/+6) values. The (somewhat localized) f-electron counts, on the other hand, can be considered a more reliable measure of actinide atomic configuration. When the atoms were allowed to relax within the GGA formalism, the magnetic moments dropped to zero in all subsequent calculations and the U electronic configuration reduced to $5f^{2.2}6d^{0.73}$. It is worthwhile to comment on procedural details of atomic and spin relaxation, because the results (vanishing moment) may be surprising. First, the atomic coordinates were determined (GGA) without the inclusion of spin. After reduction of the forces to below 0.02 eV/Å, spin polarization was enabled and the atomic positions were allowed to continue relaxing to the lowest energy structure. The atoms moved by less than 0.031 Å from the crystallographically determined positions to achieve equilibrium; thus relaxation might be expected to have little effect on derived properties. Next, the initial electronic spin structure was set as antiferromagnetic with all nearest U neighbors having opposite spins and initial moment 2 μ_B. This configuration was also allowed to relax. The Cu oxidation state

dx.doi.org/10.1021/ic300172k | Inorg. Chem. 2012, 51, 6153−6163

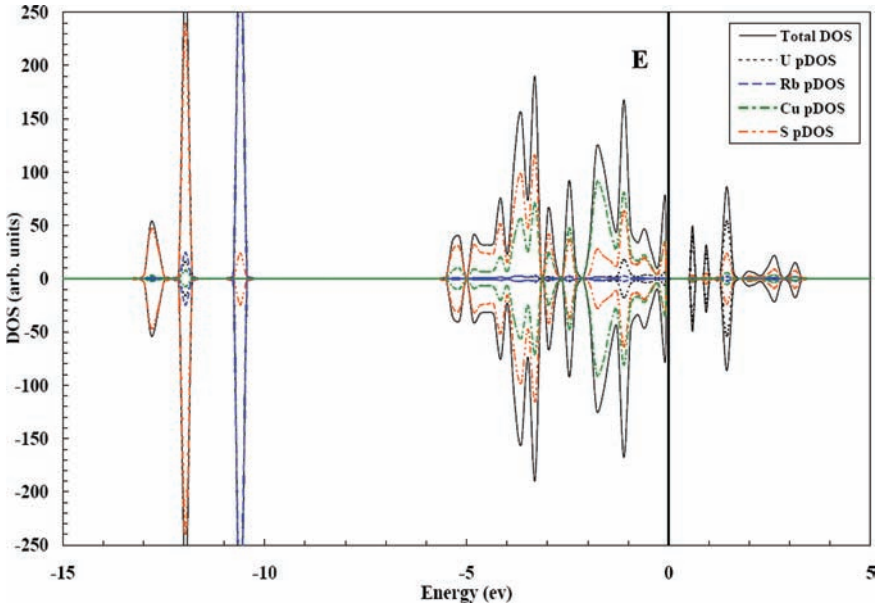

Figure 9. Total DOS and projected partial DOS for $Rb_6Cu_{12}U_2S_{15}$ from the LSDA+GGA method of DFT.

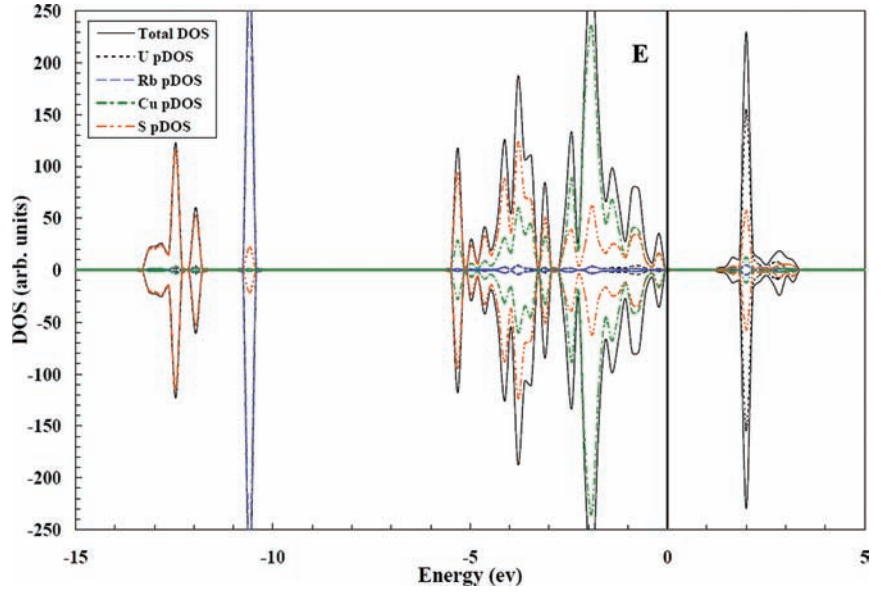

Figure 10. Total DOS and projected partial DOS for $Rb_6Cu_{12}U_2S_{15}$ using the LSDA+GGA+*U* method of DFT.

would be expected to be +1 ($3d^{10}$) and therefore without spin; nevertheless, the Cu moment was not constrained during iterations. As relaxation progressed, the spin moments diminished and essentially reached zero, suggesting a diamagnetic ground state.

With the application of 1, 2, and 4 eV on-site Coulomb corrections to the U 5f orbitals in the GGA+*U* method, the energy gap between occupied and vacant f-states increased, thus affecting the predicted optical gap (see below). The results are nontrivial owing to the simultaneous presence of 5f-6dp hybridization and U−S covalency. Consequently, the 5f-occupancy decreased, with an electronic configuration $6d^{0.73}5f^{1.2}$ found for the extreme value $U = 4$ eV, corresponding well to the U^{5+} $5f^1$ configuration suggested in previous work.[27,28]

Density of States Analysis and Optical Gap. The total density of states (DOS) and partial density of states (pDOS) resulting from the GGA and GGA+*U* models are plotted in Figures 9 and 10, respectively. The Fermi energy, E_F, has been set to zero in the diagrams. Corresponding to the experimentally determined semiconductor-like behavior, both models show band gaps of 0.68 and 1.53 eV, respectively, measured from the top of the valence band, VB, to the bottom of the conduction band, CB. The GGA (ground state) method predicts a band gap very close to that found optically of approximately 0.55 eV. It is interesting that the GGA method predicts a band gap at all; many times it fails to split the U-5f orbitals correctly and predicts wide, partially filled bands at E_F. A typical example is found in the calculated DOS for $CsCuUS_3$[84] where the method determines a metallic DOS, but the experimentally determined resistivity shows semiconductor like behavior.

As noted above, the on-site Coulomb correction was only applied to the U 5f-electrons: the major effects of this

dx.doi.org/10.1021/ic300172k | *Inorg. Chem.* 2012, 51, 6153−6163

correction are the increased energy of 5f empty states, decreased occupancy as described above, and the widening of the optical band gap. The three peaks in the DOS plot above E_F within the GGA method are mainly of U 5f and S 3p character (Figure 9). The top of the valence band, VB, contains mainly S 3p states but the small peak in U density at −1.1 eV is a filled f-band of mainly f_{xyz} and $f_{z(x^2-y^2)}$ character. Both of the first two peaks above E_F at 0.6 and 0.9 eV are the antibonding f_{xyz} and $f_{z(x^2-y^2)}$ states with overlap of the other empty f-bands. The presence of those peaks suggests to us that there is a strong covalent interaction between U and S in this compound. The third peak above E_F at 1.44 eV is almost all of f_{x^3} character but again is degenerate with the other empty f-bands. The overlap of U 5f and S 3p states notwithstanding, applying the correction for electron−electron correlation makes all these states degenerate and can be seen as the single peak in Figure 10 at approximately 2 eV. The prediction of the energy gap in the material is consistent with the semiconducting charge transport properties measured for the K analogue. The large peak in the DOS at approximately −10.6 eV is the filled Rb 4p-state (considered as valence in the pseudopotential) and there is a small S contribution owing to the Rb−S interaction. The three highest binding energy peaks between −11.8 and −13.5 eV are the S 3s-states.

Charge Distribution. Bader topological analysis was applied to GGA and GGA+*U* models;[64] the results are practically identical, suggesting that only minor changes occurred in the occupied state region (redistribution and shifts within occupied bands would not be detected). The net volume charges are: Rb, Cu, U, S = 0.85, 0.44, 1.90, −0.95 e^- respectively. Thus, whereas Rb and Cu are not very far from nominal monovalent states, the U−S covalency drastically reduces the atomic charges.

Spherical volume integration with R_{WS} for Rb, Cu, U, S(1), S(2) = 1.1, 1.1, 1.35, 2.0 Å results in volume charges of 2.52, 1.66, (3.97−4.00), −2.06, −2.29 e^- respectively. These radii were chosen to exaggerate the ionic character; as a result a considerable amount of charge falls outside the integration volumes and is not counted. Aside from the obviously truncated volume and extreme charge thus attributed to Rb, we notice that even with a small value of R = 1.35 Å for U, a net charge of only $4e^-$ is found, thus eliminating any formal hexavalent model. The structurally distinct S1 and S2 sites are resolved in this analysis, with significantly different charges correlated with their different coordination characteristics. This S1 and S2 variability is at least compatible with the hypothesis of intermediate-valence character U, charge compensated by S.

CONCLUSIONS

The properties and electronic structures of the $A_6Cu_{12}U_2S_{15}$ compounds are undeniably complex. The new information regarding these systems is that they are in fact semiconductors with narrow energy gaps of ∼0.55 eV. This is consistent with a valence precise description and/or carrier localization. The experimental data presented here are consistent with a hybrid description of $(A^+)_6(Cu^+)_{12}(U^{5+})_2(S^{2-})_{13}(S^-)_2$ and $(A^+)_6(Cu^+)_{12}(U^{6+})_2(S^{2-})_{15}$. The combination of these two states can explain the small paramagnetism, the energy gap, and the thermally activated behavior of the charge transport in these systems. Although the contribution from the $(A^+)_6(Cu^+)_{12}(U^{5+})_2(S^{2-})_{13}(S^-)_2$ state predicts p-type electrical conductivity it is possible that local distortions are present in the structure that may result in coupling of S atom-based holes. Although the synthetic protocol was the same among the reactions, the responses in the magnetic susceptibility data for some $K_6Cu_{12}U_2S_{15}$ batches varied from diamagnetic to weakly paramagnetic. It is possible that the concentration of S-based holes and the ratio of U^{6+}/U^{5+} changed from crystal to crystal perhaps because of slight nonstoichiometry. Additional work will be needed to fully address this issue.

The present DFT-GGA calculations indicate a strong degree of U−S covalency, a diamagnetic ground state, and a band gap close to that measured. Inclusion of on-site U 5f correlations through the GGA+*U* approach opens the optical gap as expected, and does not alter the predicted charge distributions significantly. Ionic charges calculated by R_{ws} volume integration and by Bader topological analysis yield *U* values consistently lower than demanded by the experimentally derived intermediate valence U 5+/6+ model. The predicted variability of S charge with site and symmetry is at least consistent with its proposed role as a charge compensator.

ASSOCIATED CONTENT

Supporting Information

Crystallographic CIF files for $A_6Cu_{12}U_2S_{15}$ (A = K, Rb, Cs) and crystallographic and structural results of the low-temperature phase of $K_6Cu_{12}U_2S_{15}$. This material is available free of charge via the Internet at http://pubs.acs.org.

AUTHOR INFORMATION

Corresponding Author

*E-mail: m-kanatzidis@northwestern.edu (M.G.K.), ibers@chem.northwestern.edu (J.A.I.).

Notes

The authors declare no competing financial interest.

ACKNOWLEDGMENTS

This research was supported at Northwestern University by the U.S. Department of Energy, Basic Energy Sciences, Chemical Sciences, Biosciences, and Geosciences Division and Division of Materials Sciences and Engineering Grant ER-15522 (J.A.I.), the National Science Foundation (DMR-1104965, M.G.K.) and at Argonne National Laboratory by the U.S. Department of Energy, OBES, Chemical Sciences Division, under contract DEAC02-06CH11357. The XANES work was supported by UChicago Argonne, LLC, Operator of Argonne National Laboratory. Argonne, a U.S. Department of Energy Office of Science Laboratory, is operated under Contract DE-AC02-06CH11357. PNC/XOR facilities and research at these facilities are supported by the U.S. DOE and its founding.

REFERENCES

(1) Haga, Y.; Aoki, D.; Homma, Y.; Ikeda, S.; Matsuda, T. D.; Yamamoto, E.; Sakai, H.; Tatejwa, N.; Dung, N. D.; Nakamura, A.; Shiokawa, Y.; Onuki, Y. *J. Alloys Compd.* **2008**, *464*, 47−50.

(2) Ott, H. R.; Rudigier, H.; Fisk, Z.; Smith, J. L. *Phys. Rev. Lett.* **1983**, *50*, 1595−1598.

(3) Sarrao, J. L.; Morales, L. A.; Thompson, J. D.; Scott, B. L.; Stewart, G. R.; Wastin, F.; Rebizant, J.; Boulet, P.; Colineau, E.; Lander, G. H. *Nature* **2002**, *420*, 297−299.

(4) Stewart, G. R.; Fisk, Z.; Willis, J. O.; Smith, J. L. *Phys. Rev. Lett.* **1984**, *52*, 679−682.

(5) Gray, D. L.; Backus, L. A.; von Nidda, H. A. K.; Skanthakumar, S.; Loidl, A.; Soderholm, L.; Ibers, J. A. *Inorg. Chem.* **2007**, *46*, 6992−6996.

(6) Rodier, N.; Tien, V. *Acta Crystallogr., Sect. B* **1976**, *32*, 2705−2707.
(7) Wells, D. M.; Jin, G. B.; Skanthakumar, S.; Haire, R. G.; Soderholm, L.; Ibers, J. A. *Inorg. Chem.* **2009**, *48*, 11513−11517.
(8) Wells, D. M.; Skanthakumar, S.; Soderholm, L.; Ibers, J. A. *Acta Crystallogr., Sect. E: Struct. Rep. Online* **2009**, *65*, I14.
(9) Yao, J. Y.; Wells, D. M.; Chan, G. H.; Zeng, H. Y.; Ellis, D. E.; Van Duyne, R. P.; Ibers, J. A. *Inorg. Chem.* **2008**, *47*, 6873−6879.
(10) Bugaris, D. E.; Ibers, J. A. *Dalton Trans.* **2010**, *39*, 5949−5964.
(11) Chan, B. C.; Hess, R. F.; Feng, P. L.; Abney, K. D.; Dorhout, P. K. *Inorg. Chem.* **2005**, *44*, 2106−2113.
(12) Choi, K. S.; Kanatzidis, M. G. *J. Solid State Chem.* **2001**, *161*, 17−22.
(13) Patschke, R.; Breshears, J. D.; Brazis, P.; Kannewurf, C. R.; Billinge, S. J. L.; Kanatzidis, M. G. *J. Am. Chem. Soc.* **2001**, *123*, 4755−4762.
(14) Mizoguchi, H.; Gray, D.; Huang, F. G.; Ibers, J. A. *Inorg. Chem.* **2006**, *45*, 3307−3311.
(15) Choi, K. S.; Patschke, R.; Billinge, S. J. L.; Waner, M. J.; Dantus, M.; Kanatzidis, M. G. *J. Am. Chem. Soc.* **1998**, *120*, 10706−10714.
(16) Folmer, J. C. W.; Jellinek, F. *J. Less-Common Met.* **1980**, *76*, 153−162.
(17) Hartig, N. S.; Dorhout, P. K.; Miller, S. M. *J. Solid State Chem.* **1994**, *113*, 88−93.
(18) Stoll, P.; Nather, C.; Jess, I.; Bensch, W. *Acta Crystallogr., Sect. C: Cryst. Struct. Commun.* **1999**, *55*, 286−288.
(19) Brown, D. B.; Zubieta, J. A.; Vella, P. A.; Wrobleski, J. T.; Watt, T.; Hatfield, W. E.; Day, P. *Inorg. Chem.* **1980**, *19*, 1945−1950.
(20) Ghosh, B. P.; Chaudhury, M.; Nag, K. *J. Solid State Chem.* **1983**, *47*, 307−313.
(21) Peplinski, Z.; Brown, D. B.; Watt, T.; Hatfield, W. E.; Day, P. *Inorg. Chem.* **1982**, *21*, 1752−1755.
(22) Julien, R.; Rodier, N.; Tien, V. *Acta Crystallogr., Sect. B: Struct. Sci.* **1978**, *34*, 2612−2614.
(23) Stowe, K. *Z. Anorg. Allg. Chem.* **1996**, *622*, 1419−1422.
(24) Briggs Piccoli, P. M.; Abney, K. D.; Schoonover, J. D.; Dorhout, P. K. *Inorg. Chem.* **2001**, *40*, 4871−4875.
(25) Chondroudis, K.; Kanatzidis, M. G. *J. Am. Chem. Soc.* **1997**, *119*, 2574−2575.
(26) Bugaris, D. E.; Choi, E. S.; Copping, R.; Glans, P. A.; Minasian, S. G.; Tyliszczak, T.; Kozimor, S. A.; Shuh, D. K.; Ibers, J. A. *Inorg. Chem.* **2011**, *50*, 6656−6666.
(27) Sutorik, A. C.; Patschke, R.; Schindler, J.; Kannewurf, C. R.; Kanatzidis, M. G. *Chem.—Eur. J.* **2000**, *6*, 1601−1607.
(28) Schilder, H.; Speldrich, M.; Lueken, H.; Sutorik, A. C.; Kanatzidis, M. G. *J. Alloys Compd.* **2004**, *374*, 249−252.
(29) Feher, F. *Handbuch der Präparativen Anorganischen Chemie*; F. Enke: Stuttgart, Germany, 1954.
(30) Jin, G. B.; Ibers, J. A. Crystallographic data for $RbCuS_4$: orthorhombic, *Fdd*2, a = 13.109(10) Å, b = 33.87(2) Å, c = 5.401(4) Å, V = 2398(3) Å^3, Z = 16. In 2011.
(31) Rüdorff, W.; Schwarz, H. G.; Walter, M. *Z. Anorg. Allg. Chem.* **1952**, *269*, 141−152.
(32) Roberts, H. S.; Ksanda, C. J. *Am. J. Sci.* **1929**, *17* (Series5), 489−503.
(33) Zachariasen, W. H. *Acta Crystallogr.* **1949**, *2*, 291−296.
(34) Suski, W.; Gibiński, T.; Wojakowski, A.; Czopnik, A. *Phys. Status Solidi A* **1972**, *9*, 653−658.
(35) *SMART Version 5.054 Data Collection and SAINT-Plus Version 6.45a Data Processing Software for the SMART System*; Bruker Analytical X-Ray Instruments, Inc.: Madison, WI, 2003.
(36) Sheldrick, G. M. *Acta Crystallogr., Sect. A* **2008**, *64*, 112−122.
(37) Sheldrick, G. M., *SADABS*; University of Göttingen: Göttingen, Germany, 2008.
(38) *X-AREA*; STOE & Cie GmbH, IPDS Software: Darmstadt, Germany, 2006.
(39) Sheldrick, G. M. *SHELXTL*, Version 6.14; Bruker Analytical X-Ray Instruments, Inc.: Madison, WI, 2003.
(40) Gelato, L. M.; Parthe, E. *J. Appl. Crystallogr.* **1987**, *20*, 139−143.
(41) Gray, D. L.; Backus, L. A.; von Nidda, H.-A. K.; Skanthakumar, S.; Loidl, A.; Soderholm, L.; Ibers, J. A. *Inorg. Chem.* **2007**, *46*, 6992−6996.
(42) Almond, P. M.; Skanthakumar, S.; Soderholm, L.; Burns, P. C. *Chem. Mater.* **2007**, *19*, 280−285.
(43) Bray, T. H.; Skanthakumar, S.; Soderholm, L.; Sykora, R. E.; Haire, R. G.; Albrecht-Schmitt, T. E. *J. Solid State Chem.* **2008**, *181*, 493−498.
(44) Rundle, R. E.; Baenziger, N. C.; Wilson, A. S.; McDonald, R. A. *J. Am. Chem. Soc.* **1948**, *70*, 99−105.
(45) Zachariasen, W. H. *Acta Crystallogr.* **1948**, *1*, 265−268.
(46) Ravel, B.; Newville, M. *J. Synchrotron Radiat.* **2005**, *12*, 537−541.
(47) Kotiim, G. *Reflectance spectroscopy*; Springer-Verlag: New York, 1969.
(48) (a) Tandon, S. P.; Gupta, J. P. *Phys. Status Solidi B* **1970**, *38*, 363−367. (b) Kanatzidis, M. G.; McCarthy, T. J.; Tanzer, T. A.; Chen, L. H.; Iordanidis, L.; Hogan, T.; Kannewurf, C. R.; Uher, C.; Chen, B. X. *Chem. Mater.* **1996**, *8*, 1465−1474. (c) Liao, J. H.; Kanatzidis, M. G. *Chem. Mater.* **1993**, *5*, 1561−1569. (d) Trikalitis, P. N.; Rangan, K. K.; Bakas, T.; Kanatzidis, M. G. *J. Am. Chem. Soc.* **2002**, *124*, 12255−12260.
(49) Wendlandt, W. W.; Hecht, H. G. *Reflectance Spectroscopy*; Interscience Publishers: New York, 1966.
(50) Kresse, G.; Furthmuller, J. *Phys. Rev. B* **1996**, *54*, 11169−11186.
(51) Kresse, G.; Furthmuller, J. *Comput. Mater. Sci.* **1996**, *6*, 15−50.
(52) Kresse, G.; Hafner, J. *Phys. Rev. B* **1993**, *47*, 558−561.
(53) Kresse, G.; Hafner, J. *Phys. Rev. B* **1994**, *49*, 14251−14269.
(54) Kresse, G.; Joubert, D. *Phys. Rev. B* **1999**, *59*, 1758−1775.
(55) Monkhorst, H. J.; Pack, J. D. *Phys. Rev. B* **1976**, *13*, 5188−5192.
(56) Hubbard, J. *Proc. R. Soc. London, Ser. A* **1963**, *276*, 238−257.
(57) Dudarev, S. L.; Botton, G. A.; Savrasov, S. Y.; Humphreys, C. J.; Sutton, A. P. *Phys. Rev. B* **1998**, *57*, 1505−1509.
(58) Gulay, L. D.; Wolcyrz, M.; Pietraszko, A.; Olekseyuk, I. D. *Pol. J. Chem.* **2006**, *80*, 1703−1714.
(59) Shick, A. B.; Pickett, W. E. *Phys. Rev. Lett.* **2001**, *86*, 300−303.
(60) de la Mora, P.; Navarro, O. *J. Phys.: Condens. Matter* **2008**, *20*, 285221/1−285221/6.
(61) Rusz, J.; Divis, M. *J. Phys.: Condens. Matter* **2004**, *16*, 6675−6684.
(62) Rusz, J.; Divis, M. *J. Magn. Magn. Mater.* **2005**, *290*, 367−370.
(63) Shannon, R. D. *Acta Crystallogr., Sect. A* **1976**, *32*, 751−767.
(64) Bader, R. F. W. *Atoms in Molecules. A Quantum Theory*; Clarendon Press: Oxford, U.K., 1990.
(65) Brochu, R.; Padiou, J.; Grandjea., D. *C. R. Acad. Sci., C, Sci. Nat.* **1970**, *271*, 642−643.
(66) Lelieveld, R.; Ijdo, D. J. W. *Acta Crystallogr., Sect. B: Struct. Sci.* **1980**, *36*, 2223−2226.
(67) Zhang, X.; Kanatzidis, M. G. *J. Am. Chem. Soc.* **1994**, *116*, 1890−1898.
(68) Yao, J. Y.; Ibers, J. A. *Acta Crystallogr., Sect. Sect. E: Struct. Rep. Online* **2004**, *60*, I118−I119.
(69) Yao, J. Y.; Deng, B.; Ellis, D. E.; Ibers, J. A. *Inorg. Chem.* **2002**, *41*, 7094−7099.
(70) Schoenes, J. *Phys. Rep.* **1980**, *66*, 187−212.
(71) Lynn, J. W.; Skanthakumar, S. Neutron scattering of lanthanide magnetic ordering. In *Handbook on the Physics and Chemistry of Rare Earths*; Gschneidner, K. A., Eyring, L., Maple, M. B., Eds.; Elsevier: New York, 2001; Vol. *31*, pp 315−350.
(72) Staub, U.; Soderholm, L. Electronic 4f state splittings in cuprates. In *Handbook on the Physics and Chemistry of Rare Earths*; Gschneidner, K. A., Eyring, L., Maple, M. B., Eds.; Elsevier Science BV: Amsterdam, The Netherlands, 2000; Vol. *30*, pp 491−545.
(73) Hinatsu, Y. *J. Solid State Chem.* **1993**, *102*, 566−569.
(74) Lea, K. R.; Leask, M. J. M.; Wolf, W. P. *J. Phys. Chem. Solids* **1962**, *23*, 1381−1405.
(75) Edelstein, N.; Brown, D.; Whittaker, B. *Inorg. Chem.* **1974**, *13*, 563−567.
(76) Hinatsu, Y. *J. Alloys Cmpds.* **1994**, *203*, 251−257.

(77) Hinatsu, Y.; Shimojo, Y.; Morri, Y. *J. Alloys Cmpds.* **1998**, *270*, 127−131.
(78) Miyake, C.; Fuji, K.; Imoto, S. *Chem. Phys. Lett.* **1977**, *46*, 349−351.
(79) Lyon, W. G.; Osborne, D. W.; Flotow, H. E.; Hoekstra, H. R. *J. Chem. Thermodyn.* **1977**, *9*, 201−210.
(80) Bickel, M.; Goodman, G. L.; Soderholm, L.; Kanellokopulos, B. *J. Solid State Chem.* **1988**, *76*, 178−185.
(81) Bickel, M.; Kanellokopulos, B. *J. Solid State Chem.* **1993**, *107*, 273−284.
(82) Hinatsu, Y.; Edelstein, N. *J. Solid State Chem.* **1994**, *112*, 53−57.
(83) Stevens, K. W. H. *Proc. Phys. Soc. London* **1952**, *A*, 209−215.
(84) Wells, D. M. Syntheses, properties, and electronic structure of materials with strongly correlated electrons. From thin film transition metal oxides to early actinide selenides. Northwestern University: Evanston, IL, 2010.

dx.doi.org/10.1021/ic300172k | *Inorg. Chem.* 2012, 51, 6153−6163